Available online at www.sciencedirect.com
ScienceDirect
Journal of Organometallic Chemistry 693 (2008) 1590–1596
Journal of Organometallic Chemistry
www.elsevier.com/locate/jorganchem

Gas phase synthesis and X-ray crystal structures of supramolecular networks with bromocorannulene: Similarities and differences with their corannulene analogs

Alexander S. Filatov, Marina A. Petrukhina *

Department of Chemistry, University at Albany, State University of New York, 1400 Washington Avenue, Albany, NY 12222, USA

Received 1 October 2007; received in revised form 9 November 2007; accepted 9 November 2007
Available online 17 November 2007

Abstract

The reactivity of bowl-shaped mono-bromocorannulene ($C_{20}H_9Br$) has been examined and compared with that of corannulene ($C_{20}H_{10}$). Although bromination of corannulene was shown to flatten the bowl and change its electronic properties, it has not affected the outcome of coordination reactions toward the avid Lewis acidic $[Rh_2(O_2CCF_3)_4]$ complex. Two new products have the same composition $[\{Rh_2(O_2CCF_3)_4\}_m \cdot (C_{20}H_9Br)_n]$ where $m{:}n = 1{:}1$ (**1**) and 3:2 (**2**), as the corresponding corannulene-based analogs. The X-ray diffraction studies of **1** and **2** revealed 1D chain and 2D layered structures built on η^2-coordination of rhodium(II) to rim carbon sites of the $C_{20}H_9Br$-bowl, similar to those of $C_{20}H_{10}$. While no essential difference is found in 2D structures, the local coordination environments of the $[Rh_2(O_2CCF_3)_4]$ unit differ in their 1D complexes.

Keywords: Bromocorannulene; Rhodium(II) trifluoroacetate; π-Arene complex; X-ray crystal structure

1. Introduction

Extensive experimental investigations into the properties and reactivity of bowl-shaped polycyclic aromatic hydrocarbons have been made possible in the last 15 years due to advances of conventional organic and gas phase (flash vacuum pyrolysis) synthetic techniques [1]. Furthermore, the use of readily available small bowls, like corannulene (Chart 1), as precursors in the synthesis of larger or functionalized non-planar polyarenes bears the enormous potential for future progress in this field [2].

In this regard, halogen derivatives of aromatic compounds are known to play an important role as common intermediates in numerous synthetic transformations. Their significance stems from the variety and reliability of nucleophilic aromatic substitution reactions that are often mediated by transition metals. For example, alkyl-, alkynyl-, and aryl-substituted corannulenes have been prepared from bromo-substituted corannulenes by Ni-catalyzed alkylations [3], Sonogashira reactions [4], and Suzuki couplings [5], respectively. Mono-bromocorannulene (Chart 1) has also been a useful intermediate for the first bowl-shaped benzyne, corannulyne, which for a long time remained an elusive target [6]. Despite this wide utilization of bromocorannulenes in synthetic organic chemistry, their structural and coordination studies are still lacking. The only use of bromocorannulene for the synthesis of the σ-bonded metal complex of corannulene has been recently reported [7]. Therefore, as part of our ongoing research program focused at the study of metal binding to planar and curved polyaromatic compounds [8], we attempted to test the reactivity and coordination properties of mono-bromocorannulene, $C_{20}H_9Br$. Herein we report the gas phase syntheses and X-ray crystal structures of the first π-bonded metal complexes of bromocorannulene.

* Corresponding author. Fax: +1 518 442 3462.
E-mail address: marina@albany.edu (M.A. Petrukhina).

0022-328X/$ - see front matter © 2007 Elsevier B.V. All rights reserved.
doi:10.1016/j.jorganchem.2007.11.017

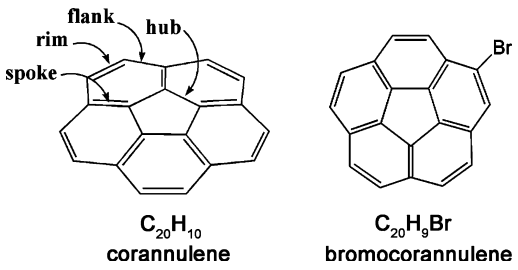

Chart 1.

2. Results and discussion

Bromocorannulene, $C_{20}H_9Br$, was synthesized from corannulene using elemental bromine and iron tribromide as a catalyst [3]. This procedure usually gives a mixture of mono- and di-bromocorannulenes that are virtually inseparable by chromatography. However, we found that sublimation of a crude product at 170–180 °C under reduced pressure (*ca.* 10^{-2} Torr) yields mono-bromocorannulene as a pure crystalline solid (yield *ca.* 90%). Unfortunately, our numerous attempts to obtain single crystals of $C_{20}H_9Br$ of sufficient quality for X-ray crystallographic studies have failed. Thus, to access geometric parameters of this bowl, DFT calculations were carried out using the hybrid Perdew–Burke–Ernzerhof parameter free exchange-correlation hybrid functional (PBE0) [9]. PBE0 was recently proven to show consistently superior results over the commonly used B3LYP functional for calculations of curved polyaromatic hydrocarbons [10] and their metal complexes [11]. DFT results have shown that bromination of corannulene flattens the bowl core. Thus, the bowl depth of $C_{20}H_9Br$ is 0.862 Å vs. that of 0.870 Å for $C_{20}H_{10}$ calculated with the same level of theory [12]. Consequently, the two possible enantiomers of bromocorannulene are rapidly converting into each other via bowl-to-bowl inversion and cannot be distinguished in solution. The energy barrier for the conversion of $C_{20}H_9Br$ is estimated to be 9.22 kcal/mol, which is 1 kcal/mol less than that for the parent $C_{20}H_{10}$-molecule. However, in the solid-state this conversion is frozen, both enantiomers co-exist and show up as a statistical mixture in the crystal structures.

The frontier molecular orbitals (FMOs) of corannulene and bromocorannulene are very similar to each other (Fig. 1); however, FMOs of $C_{20}H_9Br$ are no longer degenerate. In addition, the HOMO–LUMO band gap is decreased from 0.1728 to 0.1683 hartrees on going from $C_{20}H_{10}$ to $C_{20}H_9Br$. It is noteworthy that the electron density of bromocorannulene's HOMO is mostly localized over the corannulene core with only some residual density located at the bromine atom. This additional electron density provided by bromine to the corannulene core is predominantly distributed over all non-adjacent rim carbon atoms and does not affect interior carbon atoms (Fig. 2). Subsequently, the bond orders of only rim carbon–carbon sites are increased, while the bond orders between interior carbon atoms remain unchanged.

In a view of increased basicity of bromocorannulene, we were interested to test its reactivity toward an avid Lewis acidic dimetal complex, $[Rh_2(O_2CCF_3)_4]$, and compare it with the previously reported coordination of corannulene [13]. Synthesis of the title complexes was accomplished by sublimation–deposition reactions of the volatile, complementary donor and acceptor partners, namely $C_{20}H_9Br$ and $[Rh_2(O_2CCF_3)_4]$. Two new products $[\{Rh_2(O_2CCF_3)_4\}_m \cdot (C_{20}H_9Br)_n]$ ($m{:}n = 1{:}1$ (**1**) and 3:2

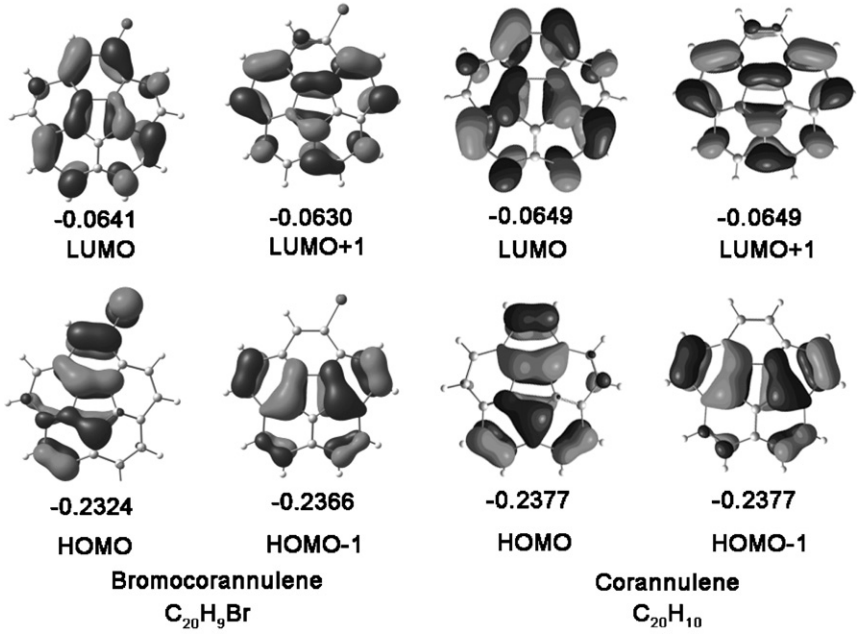

Fig. 1. Frontier molecular orbitals for corannulene and bromocorannulene. Energy units are given in hartrees. A hartree is equal to 627.51 kcal/mol.

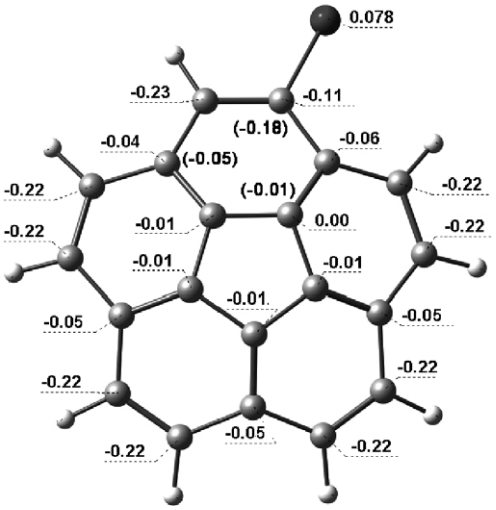

Fig. 2. Natural charge distribution in bromocorannulene and corannulene (in brackets).

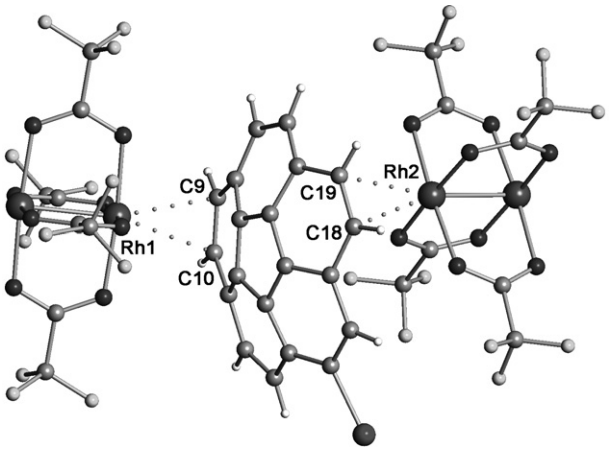

Fig. 3. A fragment of structure **1** showing the coordination of dirhodium units to both surfaces of bromocorannulene. Rh1–C9 2.537(8), Rh1–C10 2.600(9), Rh2–C19 2.598(8), Rh2–C18 2.582(9) Å.

(**2**)) have been isolated from two separate reactions performed under reduced pressure at 180–205 °C. The composition of the products was controlled by varying the reagent ratios in the solid-state. An excess of ligand in the starting mixture (Rh_2:L = 1:2) favored the formation of product **1**, which was isolated in the form of green needle-shaped crystals in 30–35% yields. On the other hand, an excess of the dimetal complex (Rh_2:L = 3:1) resulted in deposition of very dark-green blocks of **2** in 60–65% yields. Both products are sensitive to moisture with the crystals of **2** being much more stable than those of **1**. When crystals of **1** and **2** are dissolved in chloroform, they slowly dissociate into starting materials releasing free bromocorannulene and dirhodium(II, II) tetratrifluoroacetate, as confirmed by ^1H and ^{19}F NMR spectroscopy. The IR spectra of **1** and **2** in the solid-state are nearly identical and both show the presence of bromocorannulene and $[Rh_2(O_2CCF_3)_4]$ units.

The X-ray diffraction studies of $[Rh_2(O_2CCF_3)_4 \cdot (C_{20}H_9Br)]$ (**1**) and $[\{Rh_2(O_2CCF_3)_4\}_3 \cdot (C_{20}H_9Br)_2]$ (**2**) have revealed two different structural types. Compound **1** is a one-dimensional (1D) polymer consisting of alternating dirhodium tetratrifluoroacetate units and bromocorannulene molecules. Two crystallographically independent rhodium atoms of the dimetal unit each have bonding contacts with two carbon atoms of a bowl (Fig. 3).

Rh1 coordinates the ligand from the convex (*exo*) side of the bowl, while Rh2 binds from the concave (*endo*) side. Both rhodium atoms interact with the rim carbon–carbon bonds of bromocorannulene in an η^2 coordination mode. The average Rh–C separation is slightly (*ca.* 0.02 Å) shorter for the rhodium atom at the convex surface of the bowl (2.569(8) Å for Rh1; 2.590(8) Å for Rh2). There is a noticeable difference between the two Rh–C bond lengths ($\Delta = 0.063$ Å) for the Rh1 atom coordinated to the convex surface, while the bond lengths for the Rh2 atom bound to the concave surface are close ($\Delta = 0.016$ Å).

In the $[Rh_2(O_2CCF_3)_4]$ complex with corannulene of the same 1:1 composition [13], the average Rh–C distance is longer by *ca.* 0.07 Å for the rhodium atom that binds the bowl from the convex side. At the same time, the average Rh–C distances to the concave rim sites are close in the two 1D polymers. The additional electron density provided by a bromine atom to the rim bonds of $C_{20}H_9Br$ is most likely responsible for the above strengthening of the Rh–C bonding to the convex bowl surface in **1**. This also reflected in flattening of the bowl upon coordination that is more pronounced in the bromocorannulene product ($\Delta = 0.56$ Å) compared with the corannulene analog ($\Delta = 0.30$ Å).

It should be mentioned here that no metal coordination to the bromine site of $C_{20}H_9Br$ is found in the structure of **1**. In contrast, when the same dirhodium complex was reacted with 1, 3, 5-tribromobenzene, the 1D polymer $[Rh_2(O_2CCF_3)_4 \cdot (C_6H_3Br_3)]_\infty$ based on direct Rh–Br interactions has been isolated [14]. Two bromine atoms of $C_6H_3Br_3$ were involved in metal coordination with an average Rh–Br distance of 2.713(1) Å. This implies that an appreciable amount of electron density from the bromine atom is delocalized over the polyaromatic carbon surface in $C_{20}H_9Br$ dictating the above difference in coordination. This explanation is supported by the recent spectroscopic and theoretical studies showing significant π-spin density delocalization onto the bowl core for several neutral corannulene-based radicals [15].

The two analogous one-dimensional polymers based on corannulene and bromocorannulene have the same composition and the same extended structures built on weak η^2-coordination of electrophilic Rh(II) centers to the identically positioned rim C=C bonds of the bowl core. As we have recently illustrated, the topology of the FMOs of reacting partners predetermines coordination of metal centers to specific sites of aromatic ligands [16]. In this regard, the formation of identical local structures is not surprising taking into account similarities between the frontier molecular orbitals

of corannulene and bromocorannulene. However, a close inspection of the packing of alternating dimetal units and bowl-shaped ligands along the backbone of the polymeric chains revealed a difference in these otherwise very similar 1D structures (Fig. 4).

In the corannulene-based complex, each dirhodium unit is coordinated to both convex (*exo*) and concave (*endo*) surfaces of the bowl, while there is an exclusive coordination of dirhodium units to only convex or concave surfaces of $C_{20}H_9Br$ in **1**. Our DFT calculations showed that $[Rh_2(O_2CCF_3)_4]$ has a slight preference for complexation to the concave surface of corannulene [17]. This may slightly shift a statistical distribution of monomeric complexes toward the endo-bound species, $[Rh_2(O_2CCF_3)_4 \cdot (C_{20}H_{10})_{endo}]$, in the gas phase. The latter then crystallize from vapor to afford a 1D polymeric structure shown in Scheme 1a.

The bromocorannulene bowl is shallower, and that should make the *exo*/*endo* coordination preferences to be less pronounced. As a result, a 50:50 distribution of the $[Rh_2(O_2CCF_3)_4 \cdot (C_{20}H_9Br)_{endo}]$ and $[Rh_2(O_2CCF_3)_4 \cdot (C_{20}H_9Br)_{exo}]$ units in the gas phase can be expected. A different gas phase composition is then responsible for the realization of a different local solid-state structure of the bromocorannulene product (Scheme 1b).

We have also performed the reaction between $[Rh_2(O_2CCF_3)_4]$ and bromocorannulene using an excess of the former, since this was known to favor a formation of the 2D complex in the corannulene case [13]. Besides, we were interested to check if a bromine atom can be forced to react with the electrophilic rhodium(II) centers. These reaction conditions resulted in a new type of crystals for the bromocorannulene system as well. The X-ray diffraction study of the product **2** revealed that three dirhodium units are bound to the corannulene core of $C_{20}H_9Br$ in an η^2 fashion and show no coordination to a bromine atom (Fig. 5).

Each bromocorannulene molecule in **2** is coordinated twice from the convex side and once from the concave surface. As in **1**, only rim carbon atoms of the bowl are involved in coordination to the rhodium atoms. There is

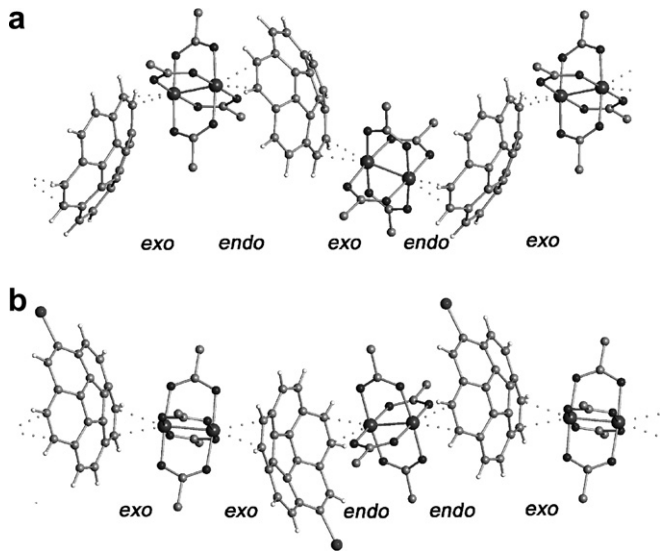

Fig. 4. Fragments of 1D infinite chains. (a) $[Rh_2(O_2CCF_3)_4 \cdot (C_{20}H_{10})]_\infty$ [13]; (b) $[Rh_2(O_2CCF_3)_4 \cdot (C_{20}H_9Br)]_\infty$. Convex (*exo*) and concave (*endo*) coordination surfaces are labeled for each dirhodium unit. Fluorine atoms are removed for clarity.

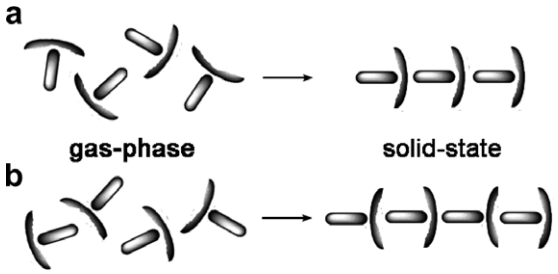

Scheme 1. Schematic representation of the formation of 1D polymers with corannulene (a) and bromocorannulene (b). $[Rh_2(O_2CCF_3)_4]$ is represented as a rectangle, while bowls are shown as curved lines.

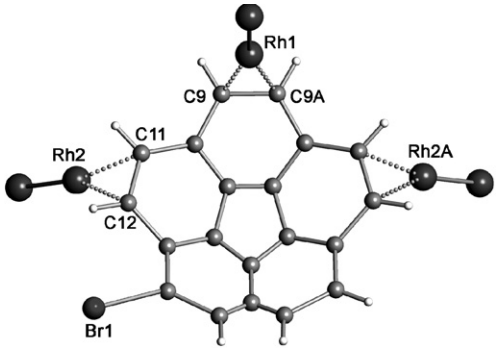

Fig. 5. A view of bromocorannulene showing the three coordinated dirhodium units in **2**. Only Rh-atoms of the latter are shown, while trifluoroacetate groups are removed for clarity. Rh1–C9 2.57(2), Rh1–C9A 2.57(2), Rh2–C11 2.56(2), Rh2–C12 2.79(2) Å.

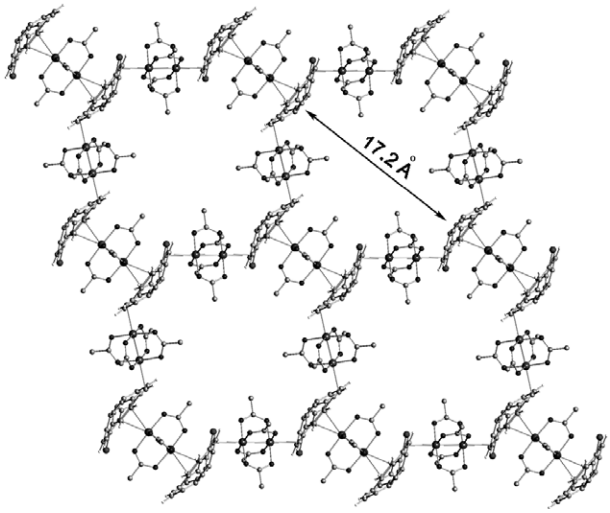

Fig. 6. A fragment of the 2D layer in **2**. Fluorine atoms are omitted for clarity.

a difference between the two Rh–C bond lengths ($\Delta =$ 0.23 Å) for the Rh2 atom coordinated to the convex surface, while the bond lengths for the Rh1 atom bound to the concave surface are exactly the same. Unlike complex **1**, an average Rh–C separation is shorter (*ca.* 0.12 Å) for the rhodium atom approaching a bowl from the concave surface (2.56(2) Å for $Rh1_{endo}$; 2.68(2) Å for $Rh2_{exo}$). In a solid state, compound **2** has an infinite 2D layered structure that is identical to that of the previously reported corannulene network (Fig. 6). For comparison, a bowl-to bowl diagonal distance in the latter is estimated to be 17.7 Å vs. 17.2 Å in the bromocorannulene analog.

3. Conclusions

A bromination of corannulene flattens the bowl and provides some additional negative charge to the rim carbon atoms. However, this does not affect the reactivity of $C_{20}H_9Br$ toward an avid Lewis acid, dirhodium(II, II) tetratrifluoroacetate, which was previously used to probe the coordination properties of corannulene. Two new bromocorannulene-based supramolecular networks of the same composition as analogous corannulene products, namely $[Rh_2(O_2CCF_3)_4 \cdot (C_{20}H_9Br)]_\infty$ (**1**) and $[\{Rh_2(O_2CCF_3)_4\}_3 \cdot (C_{20}H_9Br)_2]_\infty$ (**2**), have been synthesized in the crystalline form. The X-ray diffraction studies of **1** and **2** revealed different structural types, 1D chain and 2D layered network, respectively. Both are built on weak but directional η^2 coordination of Rh(II) to rim carbon atoms of a bowl, similar to that of corannulene. But, unlike the corannulene-based 1D polymeric complex, each dirhodium unit is exclusively coordinated to only convex (*exo*) or concave (*endo*) surfaces of the $C_{20}H_9Br$-bowl in **1**. No metal binding to the bromine atom site occurred in each case.

4. Experimental

4.1. Materials and methods

All reactions involving preparation and handling of unligated dimetal complex $[Rh_2(O_2CCF_3)_4]$ [18] were carried out under a dinitrogen atmosphere using standard Schlenk techniques. Bromocorannulene was synthesized according to a literature procedure [3] and was resublimed under reduced pressure (*ca.* 10^{-2} Torr) at 170–180 °C twice before use. IR spectra were recorded on a Perkin Elmer FT-IR Spectrometer (Spectrum 100) in the range 4000–600 cm^{-1} using universal ATR sampling accessory. GC–MS spectra were taken on HP 6890 Mass Spectrometer with Mass Selective Detector using a HP 19091J-433 column for gas chromatography. GC settings: 2 min at 80 °C, then ramp at 25–270 °C. NMR spectra were recorded on a Bruker Avance spectrometer at 400 MHz for proton and at 376 MHz for fluorine in $CDCl_3$ solutions. Chemical shifts for ^1H are reported relative to the residual solvent peaks or TMS, and for ^{19}F relative to the internal standard $CFCl_3$ ($\delta = 0.0$ ppm). Elemental analysis was performed by Maxima Laboratories, Ontario, Canada.

4.2. Synthesis of $[Rh_2(O_2CCF_3)_4 \cdot (C_{20}H_9Br)]_\infty$ (1) and $[\{Rh_2(O_2CCF_3)_4\}_3 \cdot (C_{20}H_9Br)_2]_\infty$ (2)

Mixtures of $[Rh_2(O_2CCF_3)_4]$ with mono-bromocorannulene were loaded in two separate glass ampoules that were sealed under vacuum (*ca.* 10^{-2} Torr). The ratios of the dirhodium complex to the ligand were 1:2 (0.03 and 0.06 mmol) and 3:1 (0.06 and 0.02 mmol) in the synthesis of **1** and **2**, respectively. The ampoules were placed in an electric furnace having a small temperature gradient along the length of the tube. The temperature was set at 205 °C in both cases. The green single crystals of **1** (needles) and **2** (blocks) were deposited in one day in the coldest parts of the ampoules where the temperature was set at 185 °C. Yield for **1**: 30–35%; for **2**: 60–65%. Anal. Calc. for $Rh_6C_{64}F_{36}O_{24}H_{18}Br_2$ (**2**): C, 29.18; H, 0.68; Br, 6.08. Found: C, 29.42; H, 0.56; Br, 6.08%.

IR data for **1** (cm^{-1}): 2957(w), 2923(w), 2853(w), 1650(s), 1465(m), 1220(s), 1168(s), 861(s), 827(w), 786(s), 736(s), 671(w); for **2** (cm^{-1}): 2955(w), 2921(w), 2850(w), 1653(s), 1465(m), 1221(s), 1181(s), 860(s), 825(m), 785(s), 737(s), 670(w).

^1H NMR (22 °C, $CDCl_3$) for **1** and **2**: δ (ppm) 8.04 (s, 1 H), 7.94 (d, $J = 8.6$ Hz, 1H), 7.87 (d, $J = 8.6$ Hz, 1H), 7.76–7.82 (m, 5H), 7.72 (d, $J = 8.6$ Hz, 1H); ^{19}F NMR (22 °C, $CDCl_3$): δ −75.0.

GC (corannulene): 12.8 min; (mono-bromocorannulene): 16.8 min MS (EI, 70 ev, bromocorannulene) *m*/*z*: 331, 330, 329, 328, 250, 249, 248, 247, 222, 164, 163, 122, 121, 111, 98.

4.3. Crystal structures determination and refinement

The X-ray diffraction experiments were carried out on a Bruker SMART APEX CCD-based X-ray diffractometer system equipped with a Mo-target X-ray tube (Kα radiation, $\lambda = 0.71073$ Å). Data were corrected for absorption effects using the empirical methods SADABS [19]. The structures were solved by direct methods and refined using the Bruker SHELXTL (Version 6.14) software package [20]. Details concerning crystal data and refinement are given in Table 1.

$[Rh_2(O_2CCF_3)_4 \cdot (C_{20}H_9Br)]_\infty$ (**1**): All non-hydrogen atoms were refined anisotropically except for the disordered fluorine atoms of the two CF_3-groups for which disorder was individually modeled over two or three rotational orientations. Bromine atom was found to be disordered over two positions and modeled with a 0.85:0.15 occupancy. All hydrogen atoms were included at idealized positions for structure factor calculations.

$[\{Rh_2(O_2CCF_3)_4\}_3 \cdot (C_{20}H_9Br)_2]_\infty$ (**2**): The corannulene core was found to be disordered. The disorder was modeled over two positions (0.5:0.5), and all carbon atoms were refined isotropically. Bromine atom is substitutionally

Table 1
Crystallographic data for $[Rh_2(O_2CCF_3)_4 \cdot (C_{20}H_9Br)]_\infty$ (**1**) and $[\{Rh_2(O_2CCF_3)_4\}_3 \cdot (C_{20}H_9Br)_2]_\infty$ (**2**)

	1	**2**
Formula	$Rh_2C_{28}F_{12}O_8H_9Br$	$Rh_6C_{64}F_{36}O_{24}H_{18}Br_2$
FW	987.08	1316.03
Crystal system	Triclinic	Monoclinic
Space group	$P\bar{1}$	$C2/m$
a (Å)	8.574(3)	17.9190(14)
b (Å)	8.951(3)	20.2097(14)
c (Å)	19.542(6)	11.1297(8)
α (°)	88.964(4)	90
β (°)	86.396(4)	98.077(2)
γ (°)	89.649(4)	90
V (Å^3)	1496.5(8)	3990.5(5)
Z	2	4
$D_{calculated}$ (g · cm^{-3})	2.191	2.191
μ (mm^{-1})	2.564	2.372
Radiation (λ, Å)	Mo Kα (0.71073)	Mo Kα (0.71073)
Temperature (K)	173(2)	173(2)
Data/Restraints/ Parameters	6261/24/475	4065/51/333
R_1^a, wR_2^b [$I > 2\sigma(I)$]	0.0683, 0.1779	0.0632, 0.1756
R_1^a, wR_2^b (all data)	0.1194, 0.2052	0.0829, 0.2028
Largest difference in peak (e E^{-3})	1.335 (0.13 Å from Rh2)	1.318 (0.04 Å from Rh1)
Quality-of-fit[c]	1.008	1.021

[a] $R_1 = \sum||F_o| - |F_c||/\sum|F_o|$.
[b] $wR_2 = [\sum[w(F_o^2 - F_c^2)^2]/\sum[w(F_o^2)^2]]^{1/2}$.
[c] Quality-of-fit $= [\sum[w(F_o^2 - F_c^2)^2]/(N_{obs} - N_{params})]^{1/2}$, based on all data.

disordered over three positions (with approximately the same occupancies), and this disorder was modeled along with the disorder of the corannulene core. The disorder of all fluorine atoms of the terminal CF_3-groups was individually modeled in each case over two or three rotational orientations. All remained atoms were refined anisotropically. All hydrogen atoms were included at idealized positions for structure factor calculations.

4.4. DFT calculations

The full geometry optimization for $C_{20}H_9Br$ was performed at the density functional theory using the hybrid Perdew–Burke–Ernzerhof parameter free exchange-correlation functional (PBE0) [9]. The standard 6-31G(d) basis sets were used for all atoms. The gradient norm for the geometry optimization was taken to be 10^{-4}. The true minima on potential energy surfaces were controlled by calculating the Hessian matrix and, as a consequence, harmonic frequencies. The lack of imaginary frequencies has indicated that the true minimum was achieved. When optimizations were completed, single-point calculations were performed using the extended 6-31G(d, p) basis sets for all atoms. The natural bond orbital analysis (NBO) [21] based on single-point calculations has been used for a detailed description of the electronic structure of $C_{20}H_9Br$. Optimized geometry configurations and molecular orbitals (0.038 a.u. isosurface) are visualized with the help of the ChemCraft program package (http://www.chemcraftprog.com). All calculations were carried out in the frame of the PC GAMESS (http://classic.chem.msu.ru/gran) version of GAMESS-US program package for quantum chemistry modeling [22].

5. Supplementary material

CCDC 661996 and 661997 contain the supplementary crystallographic data for **1** and **2**. These data can be obtained free of charge from The Cambridge Crystallographic Data Centre via www.ccdc.cam.ac.uk/data_request/cif.

Acknowledgements

The authors gratefully acknowledge the Donors of the American Chemical Society Petroleum Research Fund (PRF # 42910-AC3) and the National Science Foundation Career Award (NSF-0546945) for the support of this work.

References

[1] For recent reviews, see for example: (a) A. Sygula, P.W. Rabideau, Carbon-Rich Compounds (2006) 529;
(b) Y.-T. Wu, J.S. Siegel, Chem. Rev. 106 (2006) 4843;
(c) V.M. Tsefrikas, L.T. Scott, Chem. Rev. 106 (2006) 4868.
[2] (a) J. Mack, P. Vogel, D. Jones, N. Kaval, A. Sutton, Org. Biomol. Chem. 5 (2007) 2448;
(b) A. Sygula, F.R. Fronczek, R. Sygula, P.W. Rabideau, M.M. Olmstead, J. Am. Chem. Soc. 129 (2007) 3842.
[3] T.J. Seiders, E.L. Elliott, G.H. Grube, J.S. Siegel, J. Am. Chem. Soc. 121 (1999) 7804.
[4] C.S. Jones, E. Elliott, J.S. Siegel, Synlett 1 (2004) 187.
[5] A. Sygula, G. Xu, Z. Marcinow, P.W. Rabideau, Tetrahedron 57 (2001) 3637.
[6] A. Sygula, R. Sygula, P.W. Rabideau, Org. Lett. 7 (2005) 4999.
[7] (a) H.B. Lee, P.R. Sharp, Organometallics 24 (2005) 4875;
(b) H.B. Lee, P.R. Sharp, Abstracts of Papers, in: 233rd ACS National Meeting, Chicago, IL, United States, March 25-29, 2007, INOR-073.
[8] M.A. Petrukhina, Coord. Chem. Rev. 251 (2007) 1690.
[9] (a) J.P. Perdew, K. Burke, M. Ernzerhof, Phys. Rev. Lett. 77 (1996) 3865;
(b) J.P. Perdew, K. Burke, M. Ernzerhof, Phys. Rev. Lett. 78 (1997) 1396.
[10] (a) V. Barone, O. Hod, G.E. Scuseria, Nano Lett. 5 (2006) 2748;
(b) H.F. Bettinger, J. Phys. Chem. B 109 (2005) 6922;
(c) V. Barone, J.E. Peralta, G.E. Scuseria, Nano Lett. 5 (2005) 1830;
(d) M.P. Johansson, D. Sundholm, J. Vaara, Angew. Chem. Int. Ed. 43 (2004) 2678.
[11] (a) B. Zhu, A. Ellern, A. Sygula, R. Sygula, R.J. Angelici, Organometallics 26 (2007) 1721;
(b) A. Yu. Rogachev, Y. Sevryugina, A.S. Filatov, M.A. Petrukhina, Dalton Trans. (2007) 3871.
[12] Y. Sevryugina, A. Yu. Rogachev, E.A. Jackson, L.T. Scott, M.A. Petrukhina, J. Org. Chem. 71 (2006) 6615.
[13] M.A. Petrukhina, K.W. Andreini, J. Mack, L.T. Scott, Angew. Chem. Int. Ed. 42 (2003) 3375.
[14] X-ray crystal data for $[Rh_2(O_2CCF_3)_4 \cdot (C_6H_3Br_3)]_\infty$: $Rh_2C_{14}Br_3F_{12}O_8H_3$, $M_r = 972.71$, green plate, $0.25 \times 0.12 \times 0.10$, triclinic, space group $P\bar{1}$, $a = 8.4169(5)$, $b = 8.7306(3)$, $c = 17.416(1)$ Å, $\alpha = 77.30(1)°$, $\beta = 88.824(5)°$, $\gamma = 72.160(5)°$, $V = 1186.9(1)$ Å^3, $Z = 2$, $T = 213(2)$ K. Reflections collected: 6511, independent reflections 2981 ($R_{(int)} = 0.0839$), Gof on $F^2 = 1.058$, R_1 ($I > 2\sigma(I)$) = 0.0468,

$wR_2 = 0.1256$, R_1 (all data) = 0.0521, $wR_2 = 0.1318$. Rh1–Rh2 2.404(1), Rh1–Br1 2.700(1), Rh2–Br2 2.726(1), Rh2–Rh1–Br1 178.28(3), Rh1–Rh2–Br2 176.11(3).

[15] (a) K. Fukui, Y. Morita, S. Nishida, T. Kobayashi, K. Sato, D. Shiomi, T. Takui, K. Nakasuji, Polyhedron 24 (2005) 2326;
(b) S. Nishida, Y. Morita, T. Kobayashi, K. Fukui, A. Ueda, K. Sato, D. Shiomi, T. Takui, K. Nakasuji, Polyhedron 24 (2005) 2200;
(c) Y. Morita, S. Nishida, T. Kobayashi, K. Fukui, K. Sato, D. Shiomi, T. Takui, K. Nakasuji, Org. Lett. 6 (2004) 1397.

[16] A.S. Filatov, A. Yu. Rogachev, M.A. Petrukhina, Crystal Growth & Des. 6 (2006) 1479.

[17] A. Yu. Rogachev, M.A. Petrukhina, Unpublished results.

[18] F.A. Cotton, E.V. Dikarev, X. Feng, Inorg. Chim. Acta 237 (1995) 19.

[19] SADABS; Bruker AXS, Inc.: Madison, WI, 2001.

[20] SHELXTL, Version 6.14; Bruker AXS Inc.: Madison, WI, 2001.

[21] A.E. Reed, L.A. Curtiss, F. Weinhold, Chem. Rev. 88 (1988) 899.

[22] M.W. Schmidt, K.K. Baldridge, J.A. Boatz, S.T. Elbert, M.S. Gordon, J.H. Jensen, S. Koseki, N. Matsunaga, K.A. Nguyen, S. Su, T.L. Windus, M. Dupuis, J.A. Montgomery, J. Comput. Chem. 14 (1993) 1347.